DEVELOPMENT AND COMPARISON OF ULTRA SENSITIVE OPTICAL ABSORPTION SPECTROSCOPY TECHNIQUES EMPLOYING HIGH-FINESSE OPTICAL CAVITIES

Thesis

Submitted to

The School of Engineering of the

UNIVERSITY OF DAYTON

in Partial Fulfillment of the Requirements for

The Degree

Master of Science in Electro-Optics

By

Saffar Arjmandi

UNIVERSITY OF DAYTON

Dayton, Ohio

December 12, 2005

BUILDING AND COMPARISON OF ULTRA SENSITIVE OPTICAL ABSORPTION SPECTROSCOPY TECHNIQUES BY EMPLOYING HIGH-FINESSE OPTICAL CAVITIES AND RINGDOWN TECHNOLOGY

APPROVED BY:

Bradley D. Duncan, Ph.D.
Advisory Committee Chairman
Professor, ECE Department and
Electro-Optics Program

Peter Powers, Ph.D.
Committee Co-Chairman
Physics Department and
Electro-Optics Program

Scott R. Harris, Ph.D.
Committee Member
Research Scientist
Alliant Techsystems (ATK)

Donald L. Moon, Ph.D.
Associate Dean
Graduate Engineering Programs & Research
School of Engineering

Joseph F. Saliba, Ph.D., P.E.
Dean, School of Engineering

Abstract

DEVELOPMENT AND COMPARISON OF ULTRA SENSITIVE OPTICAL ABSORPTION SPECTROSCOPY TECHNIQUES EMPLOYING HIGH-FINESSE OPTICAL CAVITIES

Several ultra sensitive optical absorption spectroscopy techniques that employ high-finesse optical cavities and ringdown technology were implemented. Their relative performance and ease of use were then compared. The ringdown approach made it possible for a laser beam to interact with an absorbing species in a path that was effectively several kilometers long, thus dramatically increasing the measured absorption signal. This is extremely useful for detecting very weak absorption lines. Signal levels of up to 100,000 times more than the absorption signals generated after a single pass were obtained using Continuous Wave-Cavity Ringdown Spectroscopy (CW-CRDS) in the 1305-1310 nm region while detecting weak water absorption lines. The signal levels measured using Integrated Cavity Output Spectroscopy (ICOS) were up to 58,000 times stronger than the signal levels measured after single pass absorption of water traces in the atmosphere in the 1500-1520 nm region. When using the Off-Axis Integrated Cavity Output Spectroscopy (OA-ICOS) technique in the same region, the signal level was about 25,000 times more than the signal level due to single pass absorption.

Acknowledgements

I would like to thank all those who made it possible for me to participate in this great program and learning opportunity. I was granted the most ideal environment in which to learn the theory behind Electro-Optics while applying the theory in real world case applications. This was provided to me not only by the availability of equipment but also through the sincere care and mentorship of the personnel in charge of running this program. This program has given me the best opportunity to nurture my potential as a student and engineer. My very special thanks goes first to Robert Feldmann, AFRL/SNJM Branch Chief, and my advisor Dr. Bradley Duncan, University of Dayton Electro-Optics Program, who both trusted me, gave me this golden chance and always gave over 100 percent to make sure I will achieve my major goals and objectives .

I would have never been able to accomplish my goals without the mentorship, selflessness, extra encouragement, professionalism and the expertise of Dr. Peter Powers, University of Dayton Physics Department, and Dr. Scott Harris, ATK/Mission Research. The countless hours that they devoted to my progress ensured my education well-being.

I also need to sincerely thank Walter (Bert) Whitaker, Optimetrics Inc., who taught me all of the essential skills, from simple to sophisticated, needed to operate successfully in a scientific laboratory environment. My special thanks also goes to John Schmoll, also of Optimetrics Inc., who provided me with a great deal of technical support in data acquisition and processing which he did selflessly. I also need to especially thank my fellow lab rat Gary Ansell who never hesitated to give me all his support. Gary drove an extra 40 minutes to an hour everyday for an entire year, while I did not have a car, to

bring me to and from the lab. He did this without asking anything in return. It also has been an honor to be around great scientists such as Ernie Armstrong, Igor Anisimov, Larry Barnes, Tim Finegan, Dr. Ed Watson, Brian Stadler, Tim Meade, Matt Dierking, Jack Woods, Kevin Marks and many other motivated and caring scientists who set a great example for the successful future of graduate students.

I also need to thank Claudia, Bonnie, Richard, Dave Moeller, Denny and Doug Moore, for their logistical support and expertise.

Finally, I want to thank my beautiful wife Kristen and declare that I dedicate this work and project to her. She is standing so solid next to me and taking every step with me during these times of cancer. She has inspired me with so much hope and dreams that it does not leave much room for me to give. Because of this, I know I must keep the hope, faith and dream in order to continue to achieve the Ranger Objective.

Table of Contents

List of Figures

1 Introduction to Cavity Ringdown Spectroscopy and Related Sensitive Spectroscopy Techniques

1.1 Problem Statement

The ability to detect and measure extremely low concentrations of gas species in the environment is extremely important. Monitoring small changes in concentration of gases can have significant impacts for environmental monitoring, controlling industrial processes, maintaining the safety of spacecraft air supplies, and defense applications such as detecting chemical and biological agents. Spectroscopic techniques which measure absorption spectra of gas samples are able to use the unique spectral signatures of different species to determine the makeup of the sample. A direct absorption measurement made by measuring the difference in optical power entering and exiting a gas cell. The ratio of these values of a function of wavelength leads directly to a measurement of the sample spectrum. However, practical issues of detector noise, laser noise, and so on make direct absorption techniques difficult when the absorption results in an intensity variation of less than approximately 1%. The amount of a species needed in the gas cell to give rise to a 1% change in transmission is, in typical cases, on the order of parts per million (ppm) for a gas cell of less than 1 m in length.

Much higher sensitivity is required for applications where the goal is to detect very low concentrations and/or very weak absorbers, for example, detecting a chemical warfare agent at the edge of the plume. In other words, a sensor should detect a species long before the center of the plume passes over the sensor. Another example is an aircraft

patrolling an area which should be able to detect a plume even if it does not pass through the center of that plume. Sensitivities on the order of parts per billion or even parts per trillion are necessary for this kind of detection.

Another aspect of such a detection system is that it needs to operate outside of a laboratory environment. This puts practical constraints on the system such as insensitivity to alignment errors and vibrations. This thesis explores several detection schemes from this point of view, namely extremely high sensitivity while being amenable to difficult field situations.

The techniques that are considered here are all based upon cavity ring-down spectroscopy (CRDS). Techniques that use ringdown technology have opened new possibilities in this area of spectroscopy. Some of the more recent experiments have demonstrated concentration detection limits in ranges of parts per billion and parts per trillion[1]. This thesis focuses on establishing a facility that gives the Air Force Research Laboratory Sensors Directorate (AFRL/SNJM) the capability to perform comparative measurements between these types of detection techniques. The long term goal is to develop a system based on this technology that is robust, light weight, small, and highly sensitive that can be used for the purposes mentioned above.

1.2 Previous work

The development of thin dielectric films led to the ability to produce the highly reflective mirrors that were used in development of CRDS and related technologies. The origins of CRDS and related techniques go back to techniques developed for measuring the reflectivity of high reflectance mirrors used for missile guidance systems[2]. Absorption spectroscopy techniques, including CRDS, are based on the use of Beer-

Lambert law of absorption which will be discussed in more detail in chapter 3. The Beer-Lambert law shown in equation 1.1 relates the intensity of a beam propagating through a sample to the absorption cross section, number density, and path length according to

$$I = I_0 \exp\left[-\sigma NL\right], \qquad 1.1$$

where I is the resulting intensity, I_0 is the initial intensity of the light beam, σ is the absorption cross section, N is the number density of the absorbing species and L is the length of the optical path. If we consider a simple gas cell then the amount of absorption on a single pass is set by the length of the enclosure. CRDS and other techniques achieve a high sensitivity by increasing the effective path length, L. This is done using mirrors to bounce a beam back and forth within the gas cell to give a longer effective path length while maintaining the exterior dimensions of the gas cell. The simplest case is a White cell which can increase the path length by a factor of roughly 10 to 100. Cavity ringdown techniques, on the other hand, can increase the effective path length by a factor of over 1000. Additionally, spectroscopic techniques based upon the traditional Cavity Ringdown approach use measurements of the temporal decay of a laser pulse exiting the cavity instead of a direct measurement of the output intensity. This gives an advantage to CRDS over direct absorption since it makes the measurement much less sensitive to laser power fluctuations.

In CRDS, the absorption of a species in question is calculated by measuring the decay time, τ, of a resonant optical cavity. The decay time, τ, is the time that it takes for the intensity of the beam exiting the cavity to decrease by a factor of $1/e$.[3] The decay time, τ, of an optical cavity is given by equation 1.2,

$$\tau = \frac{2L}{c(\alpha L - \ln R)} \quad . \tag{1.2}$$

For the case of very high reflectivity mirrors, $R \approx 1-\delta$ and $\ln(R) \approx -\delta$, where δ is mirror loss, so that the expression for the time constant can be simplified to

$$\tau = \frac{2L}{c(\alpha L + \delta)} \quad . \tag{1.3}$$

This decay time is then just a function of the loss of the end mirrors which determines the leakage rate of light from an empty cavity, and the length which determines an effective round trip time for the laser pulse. When an absorbing species is added to the cavity the intensity decay is hastened by the additional loss introduced by the absorbing species. This scenario is depicted in Figure 1.1. These two mirrors are facing one another and separated by a length, L. A CRDS optical cavity is similar to the Fabry-Perot optical cavity except that the time history of light leaking from the cavity is considered whereas Fabry-Perot cavities are typically used in steady state where their narrow optical transmission characteristics make them useful for filtering and frequency measurements.

The frequency selectivity of optical cavities is a hindrance to cavity ringdown applications since the laser source is typically scanned across a range of frequencies in order to record the absorption spectrum. The many passes between the two mirrors effectively produces a very long (several kilometers) absorption cell. The length of the effective absorption path is strongly dependent on the mirror reflectivity, this is why extremely high reflectivity mirrors (99.9999%) are used for CRD techniques. Measuring the decay time of the cell as a function of wavelength permits a direct calculation of the

absorption of the species as a function of wavelength. If the absorption cross section σ of the species is known, it is easy to determine the number density N.

The detection sensitivity is related to our ability to measure changes in this time constant. Roughly we can gauge the sensitivity by $\alpha L \approx \delta$, so the better the ringdown mirrors the better our sensitivity. A more realistic approximation is that we have the ability to measure a change in the time constant by approximately 1 part in 100 so that the sensitivity is roughly $\delta/100$. Ringdown mirrors are typically $\delta = 10^{-3}$ or better.

In pulsed CRDS a laser pulse enters the cavity and a detector monitors the leakage of the energy at the other end of the cavity. If the cavity is empty then the loss will be only due to transmission through the mirrors. By addition of a sample gas with absorption features at the same frequency of laser the loss will be due to both transmission through the mirrors and absorption and we will observe a sharp decrease in decay time. This is the fundamental observation that gives rise to all the branches of Ringdown Technology such as CW-CRDS, Integrated Cavity Output Spectroscopy (ICOS) and Off-Axis ICOS (OA-ICOS) OA-ICOS that will be discussed in this project. These techniques have proven very useful in optical absorption measurements of atoms, molecules, and other optical components[3]. The CRDS techniques make it possible to perform very sensitive measurements with relatively simple experimental setups. This is a big reason for the recent interest that is lately given to further developing this technology.

Cavity ringdown spectroscopy can also be performed with CW lasers. In CW-CRDS intensity is a built up inside the cavity and then the laser source is rapidly switched and a detector monitors the decay time. Again, the experimental setup is basically that shown in Figure 1.1.

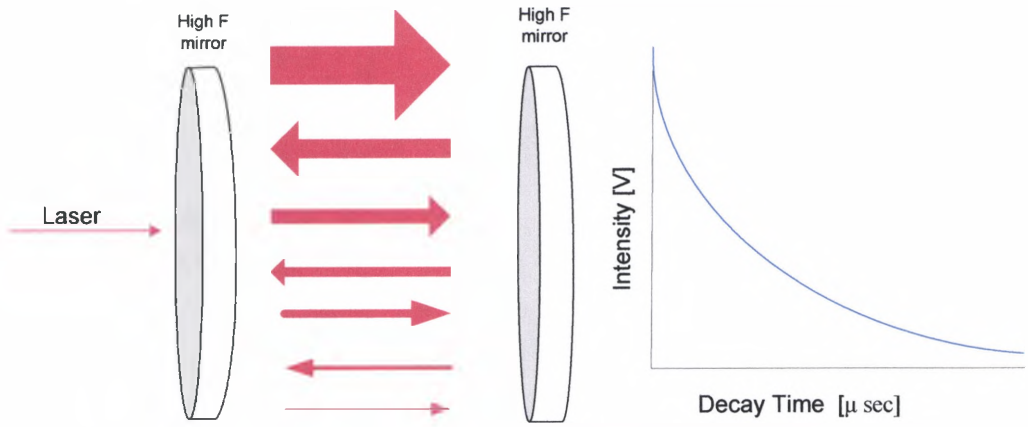

Figure 1.1. The laser is exit the cell is monitored to measure the intensity decay time. Some of the light is lost due to absorption while the rest leaks out of the mirrors and is monitored at one end by a fast detector. In a typical ringdown cell, the light travels several effective kilometers before the signal dies down. The decay times are normally on the order of microseconds.

Kevin Lehman from Princeton university was first to use continuous wave lasers for CRDS. He was able to increase the detection sensitivity as well as the resolution due to the narrow line width of the CW lasers[2]. CW laser sources for CRDA are usually based on laser diodes are generally much less expensive and more compact than the pulsed laser systems. The CW-CRDS system, however, requires careful mode-matching of the laser to the ring-down cavity. This requirement is somewhat problematic for a rugged, fielded system.

Another technique which is less sensitive to alignment is the Integrated Cavity Output Spectroscopy (ICOS) technique. Anthony O'Keefe with his group from Los Gatos Research Labs and G. Meijer and his colleagues in Netherlands have accomplished some of the most extensive work in the area of ICOS, also known as Cavity Enhanced Absorption Spectroscopy (CEAS). This technique is nearly the same as CRDS except that the laser frequency is not locked to the ringdown cavity and the output intensity of

the cavity is monitored instead of the temporal characteristics. The main advantage of ICOS in comparison with CRDS is in its simplicity. For example, ICOS does not need accurate mode matching and yet it produces accurate and sensitive absorption measurements. By introducing cavity length perturbations and small laser wavelength changes the cavity is driven in and out of resonance with the laser, averaging out the frequency selective Fabry-Perot characteristics of the cavity. By integrating over a relatively long time the probability is that the cavity becomes excited many times. The result is for any integration time, several ringdown 'spikes' occur. The area of the ringdown spikes is proportional to the loss so that for a representative integration time, the integrated signal then corresponds to the loss. Because the total intensity of the output is monitored, a slow, large area can be used instead of the fast detector required by CRDS. By looking at the change in signal as the laser is tuned provides the absorption signal[4].

The ICOS technique can be further modified by considering an off-axis laser injection geometry (OA-ICOS). Herriot, Kogelnik and Kompfner in their 1964 paper showed that when an off-axis beam is injected into an optical cavity the ray will travel back and forth in an elliptical pattern. Harriot and his group found the geometrical properties necessary for the entering beam that turned the elliptical pattern to a circular pattern and caused a reentrance condition back into the cavity[5]. This effectively created a Cavity Ringdown type cell with a long path length that similar to the ICOS setup randomized the cavity modes and makes it possible to average the transmission spectrum of the cavity. Joshua B. Paul from Harvard[6] followed by several other groups used these properties to make very sensitive absorption measurements with results similar to those

obtained with CRDS and ICOS setups. OA-ICOS has the simplest setup and equipment requirement in comparison with ICOS and CRDS. Unlike CRDS there is no need for mode matching or cavity length dithering.

1.3 Thesis Overview

This thesis documents the implementation and comparison of several CRDS optical spectroscopy techniques with an emphasis on rugged and compact setups. The theory behind absorption spectroscopy, optical cavities are discussed in chapters 2. Chapter 3 describes in detail the various experimental configurations that were implemented. In chapter 4 the results of the experiments are presented and compared to the HITRAN spectral database in order to determine the sensitivities of the techniques. Finally in chapter 5 we compare the techniques with one another and discuss each techniques strength and shortcomings as far as sensitivity, cost, robustness, and simplicity from an Air Force applications point of view.

2 Optical Cavities and Mode Formation

Cavity ringdown spectroscopy and derivative techniques are all heavily dependant on understanding the modes of optical cavities. This chapter goes over the essential theory of optical cavity modes to give a complete picture of the resonator based spectroscopic techniques developed in this thesis.

2.1 Optical Cavities

An optical cavity consists of a periodic focusing action that takes place as light rays bounce back and forth between the spherical mirrors. Each pass can be described with a characteristic ABCD matrix determined by the specific optical elements. The ray transfer of n consecutive passes can be evaluated by the nth power of the ABCD matrix for a single round trip as shown in

Figure 2.1.

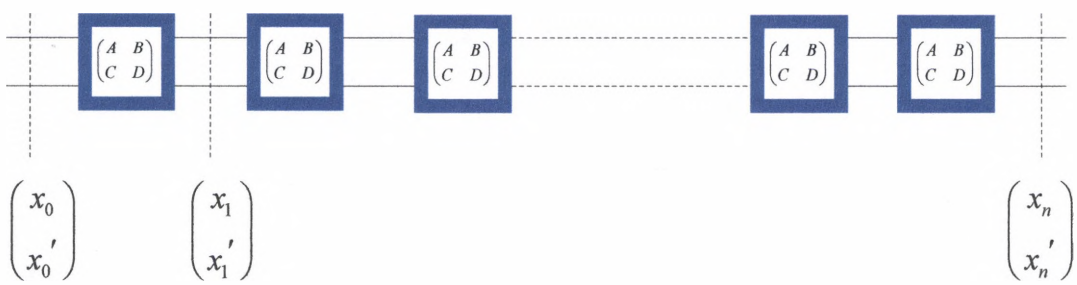

Figure 2.1. A ray in the cavity sees a periodic sequence of identical transfer matrices.

For N trips, the ray transfer matrix is

$$\begin{pmatrix} A & B \\ C & D \end{pmatrix}^N . \qquad 2.1$$

Then, in the limit as $N \to \infty$ we can use Sylvester's theorem to evaluate this matrix. We find that

$$\lim_{N\to\infty}\begin{pmatrix} A & C \\ B & D \end{pmatrix}^N = \frac{1}{\sin\theta}\begin{pmatrix} A\sin n\theta - \sin(n-1)\theta & B\sin n\theta \\ C\sin n\theta & D\sin n\theta - \sin(n-1)\theta \end{pmatrix}, \qquad 2.2$$

where $\cos\theta = \frac{1}{2}(A+D)$. This results in the stability criterion shown in equation 2.3.

$$|A+D| < 2 \qquad 2.3$$

When the cavity is unstable the rays become more and more divergent for each pass through the cavity. For ringdown systems the cavities used are particularly simple and consist of two spherical mirrors with radii of curvature R_1, R_2 and a mirror spacing d. The roundtrip ray transfer matrix is given by

$$\begin{pmatrix} 1-\frac{2d}{R_1} & 2d\left(1-\frac{d}{R_2}\right) \\ \frac{2}{R_2}-\frac{2}{R_1}+\frac{4d}{R_1R_2} & 1-\frac{2d}{R_2}-\frac{4d}{R_1}+\frac{4d^2}{R_1R_2} \end{pmatrix} = \begin{pmatrix} 1 & 0 \\ \frac{-2}{R_1} & 1 \end{pmatrix}\begin{pmatrix} 1 & d \\ 0 & 1 \end{pmatrix}\begin{pmatrix} 1 & 0 \\ \frac{-2}{R_2} & 1 \end{pmatrix}\begin{pmatrix} 1 & d \\ 0 & 1 \end{pmatrix}. \qquad 2.4$$

Therefore, the ringdown system the cavity is stable as long as

$$0 \le \left(1-\frac{d}{R_1}\right)\left(1-\frac{d}{R_2}\right) \le 1 \quad . \qquad 2.5$$

Stability is, of course, necessary for ringdown type experiments in order to achieve a large number of round trips in the cavity. Once we have a stable cavity it is then important to understand the detailed properties of the modes in the cavity in order to understand the frequency selectivity of cavity and the details of efficient coupling of a laser source into the cavity.

2.2 Modes of Optical Cavities

2.2.1 Beam modes with Cartesian Symmetry

Using a Cartesian coordinate system we assume the following trial solution to the paraxial wave equation:

$$\varphi(x,y,z) = g\left(\frac{x}{w(z)}\right)h\left(\frac{y}{w(z)}\right)\exp\left[-i\left(P(z)+\frac{k}{2q(z)}\left(x^2+y^2\right)\right)\right]. \qquad 2.6$$

By introducing g and h we allow the modes of propagation to have different horizontal and vertical functional forms. $P(z)$ is a phase shift factor which is associated with the propagation of the light beam and $q(z)$, defined in equation 2.7, is the beam parameter which is most often used to describe the propagation of a Gaussian beam.

$$\frac{1}{q} \equiv \frac{1}{R(z)} - i\frac{\lambda}{\pi w^2(z)} \qquad 2.7$$

In addition, $w(z)$ is the radius of the beam and $R(z)$ is the radius of curvature of the phase front. If we substitute the trial functional form for $\varphi(x,y,z)$ into the paraxial wave equation shown in equation 2.8, the partial differential equation reduces to an ordinary differential equation and the form of g and h can be determined.

$$\frac{\partial^2\varphi}{\partial x^2} + \frac{\partial^2\varphi}{\partial y^2} - 2ik\frac{\partial\varphi}{\partial z} = 0 \qquad 2.8$$

After some algebra, we find that

$$g\left(\frac{x}{w(z)}\right)h\left(\frac{y}{w(z)}\right) = H_m\left(\sqrt{2}\frac{x}{w(z)}\right)H_n\left(\sqrt{2}\frac{y}{w(z)}\right), \qquad 2.9$$

where H_m and H_n are Hermite polynomials of order m and n which define the transverse mode number. The first four even and odd Hermite Polynomials are shown below:

$$\left.\begin{aligned} H_0(x) &= 1 \\ H_1(x) &= 2x \\ H_2(x) &= 4x^2 - 2 \\ H_3(x) &= 8x^3 - 12x \end{aligned}\right\}, \qquad 2.10$$

The complete expression for the higher order modes is then shown in equation 2.11

$$\varphi_{n,m}(x,y,z) \propto \frac{w_0}{w(z)} H_m\left(\sqrt{2}\frac{x}{w(z)}\right) H_m\left(\sqrt{2}\frac{x}{w(z)}\right) \times \exp\left(-i\left(kz-(m+n+1)\phi\right)-\left(\frac{x^2+y^2}{w^2(z)}\right)-ik\left(\frac{x^2+y^2}{2R(z)}\right)\right), \qquad 2.11$$

where

$$\phi = \tan^{-1}\left(\frac{\lambda z}{\pi w_0^{\,2}}\right) . \qquad 2.12$$

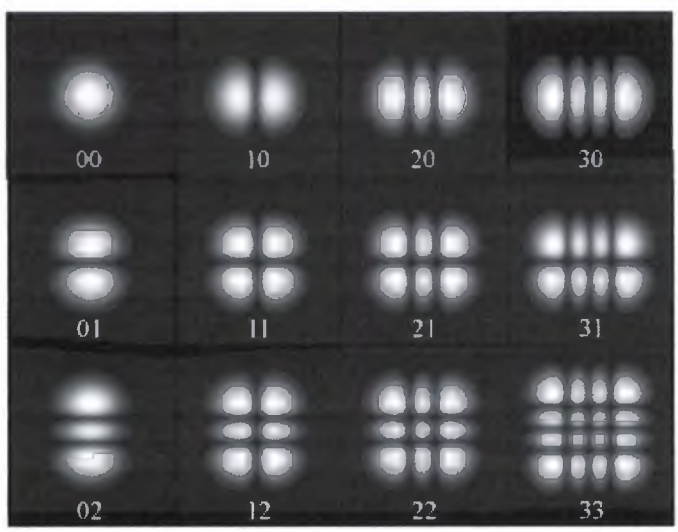

Figure 2.2. Hermite Gaussian laser mode intensity patterns[11].

The first few Hermite-Gaussian (HG) modes are shown in Figure 2.2, above. Clearly the lowest order mode is just a Gaussian beam.

It is important to notice the additional phase factor beyond that due to plane wave propagation. This part of the phase shift is shown in equation 2.13. The additional phase shift is a function of mode number and it explains why different cavity modes have different resonant frequencies.

$$\Phi(m,z,z) = (m+n+1)\tan^{-1}\left(\frac{\lambda z}{\pi w_0^{\,2}}\right) \qquad 2.13$$

For example, if one considers the TEM_{01} of a resonant cavity from a ray optics perspective, the rays trace out a bowtie in the cavity and the longer path length results in the different phase shift, and resonant frequency. In most cavity ringdown based techniques it is desirable to have a well defined cavity resonant frequency so only the lowest order mode is excited. In off axis ICOS, however, we excite a very high number of modes so that the different resonant frequencies will fill in the transmission spectrum of the cavity.

From the standpoint of CRDS, Figure 2.2 shows what the input laser beam must look like in order to couple to a cavity mode. In general, we will couple to TEM_{00} since this mode is what typical laser outputs approximate. Another note of interest is that the higher order modes extend farther from the center of the mirror and so will theoretically see more diffractive loss due to clipping on the finite cavity mirrors.

2.2.2 Cylindrically Symmetric Higher Order Beams

The optical modes of a cavity can also be expressed in a cylindrical coordinate system and their derivation follows the same path as in section 2.2.1. These cavity modes

are called Laguerre-Gaussian beams and the first few modes, designated TEM_{pl} are shown in Figure 2.3.

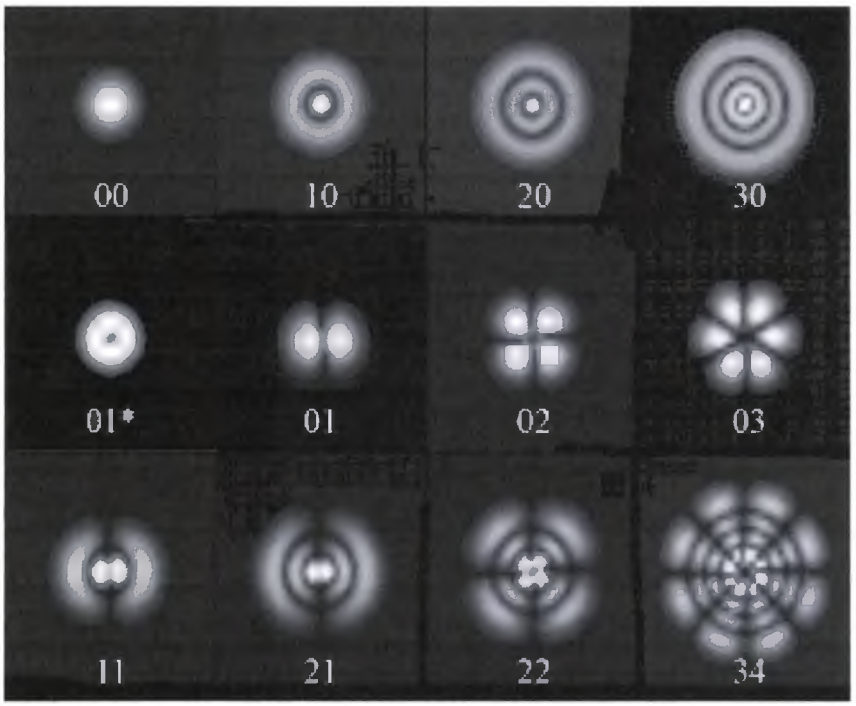

Figure 2.3. The Laguerre-Gaussian laser mode intensity patterns[11].

Regardless of the basis functions chosen to express the higher order modes, the physics remains the same and either basis set can be used to decompose more complicated cavity modes. In general, the low order Hermite-Gaussian modes are more useful since they are a better match to the modes that are excited by a small laser beam exciting a resonant cavity.

2.3 Mode Matching

Because very high reflectivity mirrors are used in CRDS techniques most of the light of the laser is simply reflected from the mirror at the cavity entrance, therefore it is important to efficiently couple the laser into the cavity by mode matching. In addition,

different cavity modes have different resonant frequencies and the excited cavity mode may change as the laser is scanned infrequency unless the modes are well matched and the overlap between the input been and the higher order modes is minimized. It is also worth noting that the different modes may have different cavity lifetimes because higher order modes clip more than the lower order modes. However, because our mirror size was many times larger than the beam diameter, such effects will not be appreciable.

In order to efficiently couple into a CRDS cell we must match the nominal Gaussian beam from the laser with the transverse mode in the cavity. The parameters of the beam injected into the CRDS cell system is usually different from the parameters of the beam inside the optical cavity. Therefore, in order to efficiently couple into the CRDS cell we must determine the parameters of the mode in the cavity, the parameters of the beam exiting the laser, and design a system of lenses to transform the laser beam into a wave front that matches that at the cavity input. Figure 2.4 shows a schematic diagram of the laser-cavity coupling arrangement.

We should also note that after much time it was realized that the CRDS mirrors initially used were not made of fused silica but of silicon, and the high index of refraction of these mirrors made the defocusing action of the mirror important to account for in the mode matching calculations.

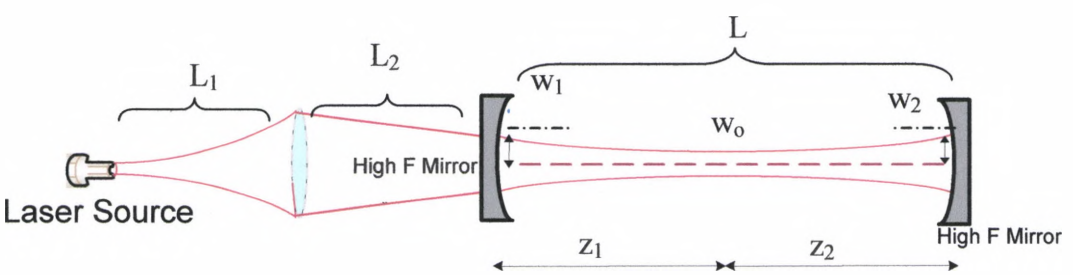

Figure 2.4. Schematic diagram of the mode matching arrangement.

3 Highly Sensitive Optical Spectroscopy

This chapter discusses the theory behind the experimental techniques that were implemented in the course of this thesis and presents expressions for their performance in a unified framework.

3.1 Absorption Spectroscopy

In direct absorption spectroscopy the absorption coefficient as a function of frequency, $\alpha(\omega)$, is obtained by measuring the change in intensity as a beam of monochromatic light as it passes through a sample of length L. The resulting change in intensity due to absorption is given by the Beer-Lambert law and is show in equation 3.1

$$I(\omega) = I_0(\omega)\exp\left[-\alpha(\omega)\right] \quad , \tag{3.1}$$

where I_0 is the initial intensity of the beam before going through the sample and $\alpha(\omega) = NL\sigma(\omega)$. In the typical case of small absorption where $\alpha \approx 1$, we can make the following approximation:

$$\exp(-\alpha) \approx 1-\alpha \, . \tag{3.2}$$

This will allow us to modify equation 3.1 to yield the following relationship

$$\frac{I(\omega)}{I_0(\omega)} = 1-\alpha(\omega), \tag{3.3}$$

or

$$\frac{\Delta I}{I} = \frac{1-a}{a} \quad , \tag{3.4}$$

where $a = 1-A = 1-\exp(-\alpha(\omega))$.

Figure 3.1 shows the experimental setup used to demonstrate absorption spectroscopy. This setup also contains several improvements over the basic absorption measurement outlined above. The absorption path, L, is made longer by bouncing the beam between several mirrors and an auto-balanced detector[24] is used to directly measure $\frac{I(\omega)}{I_0(\omega)}$. The use of the auto-balanced detector minimizes errors in the measurement caused by laser intensity noise as well as power fluctuations caused by current or temperature tuning. Typically, the intensity variation due to current tuning a diode laser will easily swamp small spectral features.

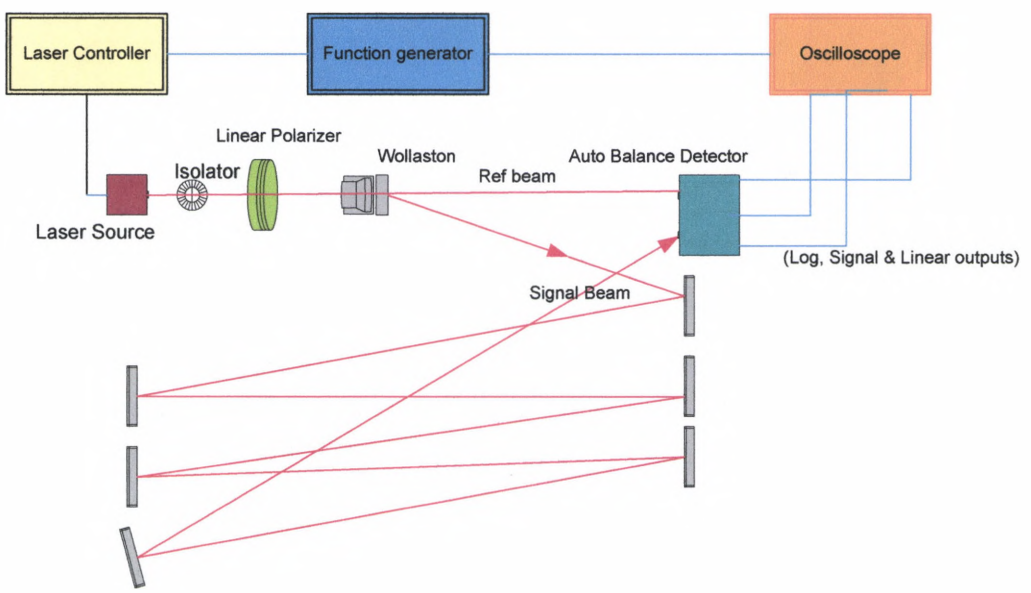

Figure 3.1. Schematic diagram of a direct absorption Spectroscopy setup that include a reference beam and auto-balanced detector.

Practically speaking we see that the absorption sensitivity is directly related to how well we can measure the laser power or intensity. A very quiet laser will allow us to measure small changes in intensity, whereas a noisy laser will be difficult to distinguish

intensity changes due to absorption versus changes due to laser fluctuations. The use of an auto-balanced detector can allow the sensitivity to approach that set by the shot noise limit, but this approach is still limited to relatively short path lengths since the multiple bounce approach quickly becomes unwieldy.

3.2 Cavity Ringdown Spectroscopy

In chapter 1 we introduced the basic concepts of the Cavity Ringdown approach. Here we give a detailed derivation for the expected signal. We will derive the differential equation for the intensity of light in an empty ringdown cavity by noting that during a roundtrip in the cavity the intracavity intensity is reduced by $I(1-R)$. Further, we can easily see that the round trip time in the cavity is L/c. If the number of round trips is large we can write a differential equation describing the intensity in the cavity as a function of time:

$$\frac{dI}{dt} \approx \frac{\Delta I}{\Delta t} = \frac{-I(1-R)}{L/c} \quad . \tag{3.5}$$

Solving equation 3.5 we see that

$$I(t) = I_0 \exp(-t/\tau), \tag{3.6}$$

where

$$\tau = \frac{L}{c(1-R)} \quad . \tag{3.7}$$

Now, τ is just the empty cavity lifetime. If there is an absorbing species in the cavity then it introduces an additional round trip loss which can be included by writing

$$R' = RA = R\exp(-\alpha(\omega)), \tag{3.8}$$

where $1-A$ is just the intensity loss during one round trip given by the Lambert-Beer law. The additional round trip loss decreases τ, which is now shown in equation 3.9.

$$\tau = \frac{L}{c(1-R')} \qquad 3.9$$

So, by simply measuring the decay time of the cavity as a function of wavelength and knowing the decay time of the empty cavity, one can easily determine the absorption as a function of wavelength. A typical ring down trace recorded in the laboratory is show in Figure 3.2, and the cell used in the CW-CRDS experiments is shown in Figure 3.3.

Although CRDS was pioneered with pulsed lasers, the low cost, small size, wide tuning range, narrow line width, and ease of use make diode lasers particularly attractive for cavity ringdown experiments. In a CW-CRD experiment, the CW laser needs to be shut off in order to view the ringdown. The ringdown is obtained by mode matching the laser into the CRDS cavity and then slowly (compared to the cavity ringdown time) scanning the length of the cavity with a piezoelectric actuator. At some point the cavity will come in to resonance with the CW laser and the transmitted signal will grow. By setting a threshold level on the detector as a trigger, the laser can be quickly turned off, deflected with an acousto-optic modulator, or shifted out of resonance by changing the diode current. No matter what approach is chosen, the laser is effectively decoupled from the cavity and a ringdown can be observed by monitoring the intensity on the detector. If the cavity length is scanned back and forth over one free spectral range in a time, Δt, we expect to measure ringdown events at a frequency of $\frac{1}{\Delta t}$. Because the maximum scanning rate for the cavity is fixed by the relative overlap of the laser line and cavity

resonance as well as the time required for the cavity intensity to build up to a detectable level, the maximum data rate is limited in this approach.

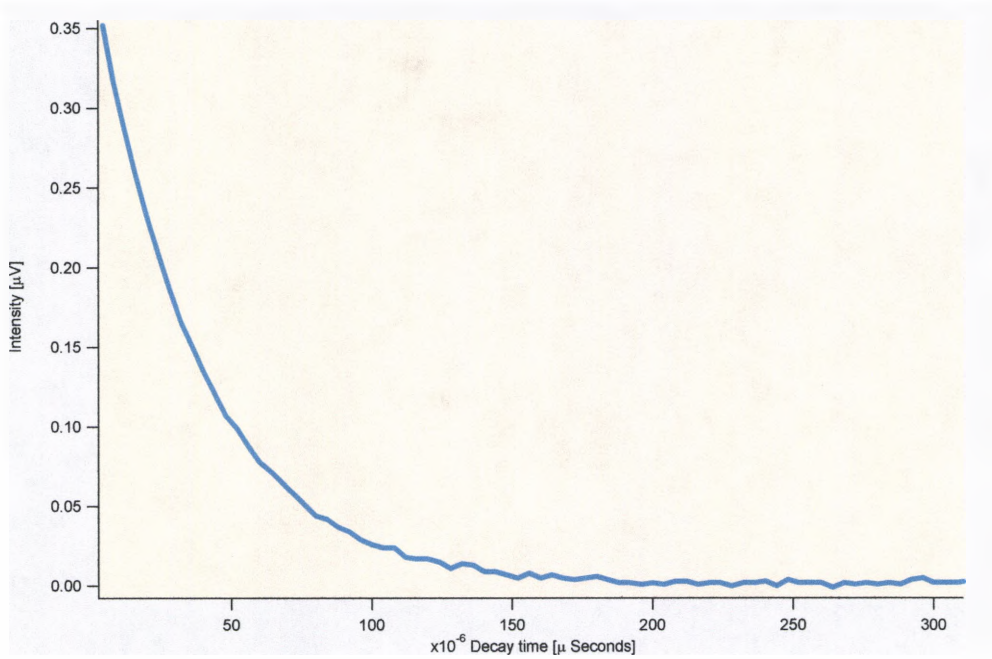

Figure 3.2. Shows a typical ringdown decay that was measured during one of CRDS experiments.

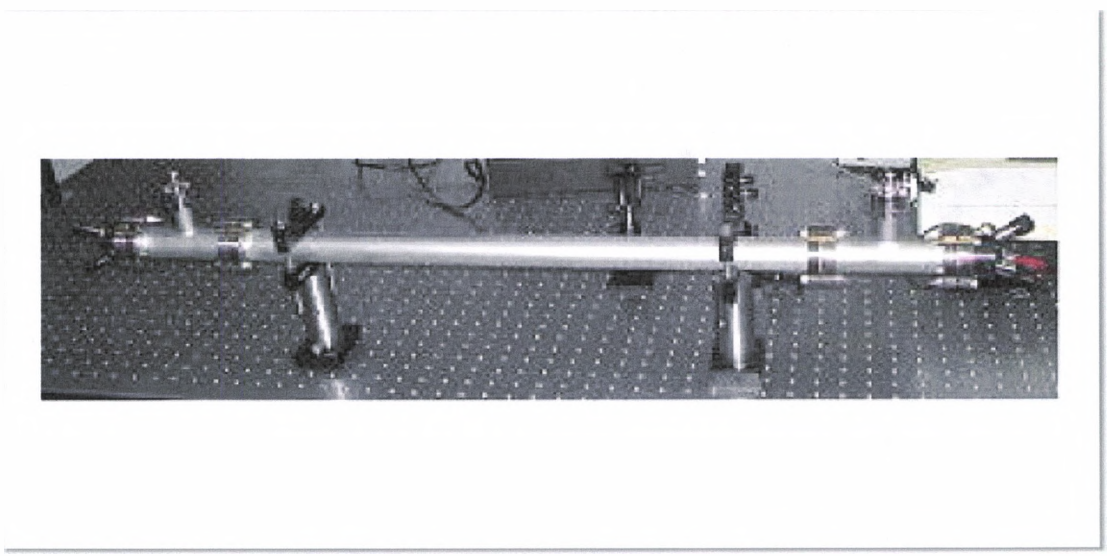

Figure 3.3. The cell used in the CW-CRDS experiments. The micrometers on the right side of the cavity included piezoelectric actuators for scanning the cavity length.

3.3 Integrated Cavity Output Spectroscopy(ICOS)

The main difference between Cavity Ringdown Spectroscopy (CRDS), which was discussed in the previous section, and Integrated Cavity Output Spectroscopy (ICOS) is that the output intensity of the cavity is monitored instead of the decay time. The mathematical analysis for ICOS proceeds exactly as for CRDS except that there is a source term added to the differential equation describing the time history of intensity inside the cavity. The modified version of equation 3.5 with the additional intensity source term is shown in equation 3.10. The source term is the laser intensity injected into the cavity, $I_L T$, modified by a cavity coupling parameter, C_p, between 0 and 1.

$$\frac{dI}{dt} \approx \frac{\Delta I}{\Delta t} = \frac{I_L C_p T/2 - I(1-R)}{L/c} \qquad 3.10$$

The factor of two in the source term is because the loss from each mirror happens twice on a round trip, but light is only injected once per round trip. The expression for the intensity exiting the cavity is shown in equation 3.11.

$$I(t) = \frac{I_L C_p T}{2(1-R)}\left[1 - \exp(-t/\tau)\right] \ , \qquad 3.11$$

where $\tau = \frac{L}{c(1-R)}$ is the unchanged time constant for the cavity. Once the empty cavity reaches steady state the intensity leaving each end mirror is just half of the light coupled into the cavity, $\frac{I_L C_p T}{2}$. Once again we replace the R in equation 3.11 with R' from

equation 3.8 so that the additional cavity loss due to absorption is included. The resulting intensity leaving the cavity in steady state is

$$I_{out}\frac{I_L C_p T}{2(1-R')}. \tag{3.12}$$

Clearly, the absorption of the cavity is encoded in the output intensity through the effect of R'. We can compute the fractional change in the output intensity by solving for $\Delta I/I$. Performing the algebras we find that

$$\frac{\Delta I}{I}=\frac{Ga}{1+Ga}\quad , \tag{3.13}$$

where $a=1-A=1-\exp\left(-\alpha(\omega)\right)$ is the absorption and G, or the cavity gain can be shown in equation 3.14 [22].

$$G=\frac{R}{1-R} \tag{3.14}$$

For small absorption, $Ga\approx 1$ so the signal is approximately

$$\frac{\Delta I}{I}\approx Ga. \tag{3.15}$$

Clearly the effect of the cavity is to amplify the changes in the output intensity by a factor of G. Figure 3.4 shows a plot of the gain factor for a range of reasonable mirror reflectivities.

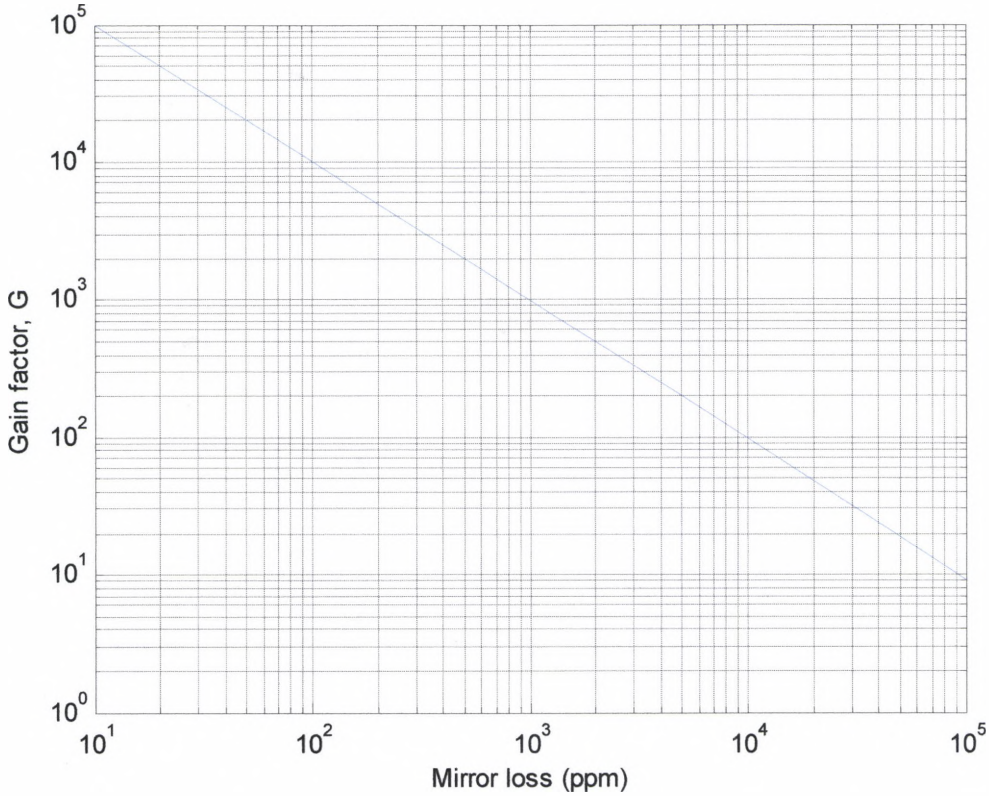

Figure 3.4. Cavity gain as a function of mirror loss.

In order to achieve the large gains that are possible with ICOS it is necessary to consider the frequency selective behavior of a resonant cavity. The obvious, but complicated experimental approach is to lock the cavity length of the cavity to the input laser frequency as it is scanned and to monitor the output intensity of the cavity. This approach is very complicated requiring a large amount of additional equipment besides a tunable laser, detector, and cavity. The approach taken here is to rapidly dither the cavity length with a piezoelectric actuator so that the length varies over one free spectral range. As a result, for every oscillation of the cavity length the laser and cavity will be inresonace at least twice. This is similar to the CW-CRDS approach described above

except that both O'Keef and Meijer have shown that the time averaged output of such an arrangement is proportional to the absorption in the cell[14,18].

The cavity length must be scanned slowly enough so that the intracvaity intensity approach steady state every time the laser frequency overlaps the cavity mode, but fast enough so that the flickering output intensity can be effectively averaged. Because there a large amount of time during each cavity length oscillation when the output is zero, the average intensity output can be quite low in this approach, however since the measurement is not a fast ringdown, a large sensitive detector can be used.

3.4 Off Axis ICOS

The Off-Axis ICOS technique is an extension of the on-axis ICOS approach that was discussed in the previous section. Instead of coupling the laser to TEM_{00}, the laser couples to the cavity by exciting a reentrant mode similar to that in a white cell. Because this mode is really the superposition of many fundamental TEM_{mn} modes, the frequency selectivity of the cavity is greatly suppressed while the effective gain of the cavity for absorption measurements is preserved. A higher order transverse TEM_{mn} mode has $(m+n)$ times smaller FSR than a TEM_{00} mode[19].

It has shown by Herriott, Kogelnik and Kompfner[20] in 1964 that when a beam is injected into the cavity with an off axis angle, the reflections off the surfaces of the cavity mirrors will lie in an elliptical or circular pattern as shown in Figure 3.5. The radius A, of the beam spots as they rotate around the cavity circumference is given by

$$y_0' = A/\sqrt{fd} \quad , \qquad 3.16$$

where f is the focal length of the cavity mirror (f=R/2). The rotation angle on each pass is given by

$$\cos\theta = 1 - d/R \qquad 3.17$$

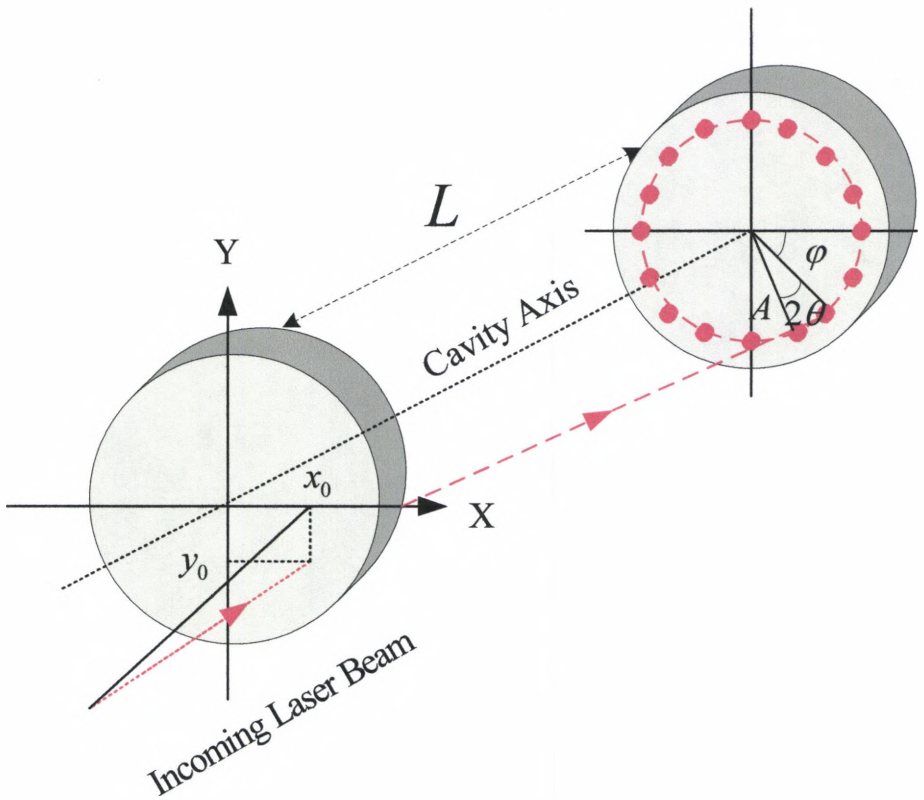

Figure 3.5. Off-axis alignment and beam propagation in an optical cavity. Figure adapted from Bakhirkin et al[19].

Further, Herriot and his group demonstrated that once the geometrical retracing condition in equation 3.19 is met, in addition to the usual cavity stability criterion in equation 3.18, then the ray will retrace its path. The cavity stability criterion is

$$0 \le \left(1 - \frac{d}{R_1}\right)\left(1 - \frac{d}{R_2}\right) \le 1 \quad , \qquad 3.18$$

where d is the spacing between the cavity mirrors, R_1 and R_2 are the radii of curvature of the cavity mirrors. In addition the re-entrance condition is satisfied when

$$2m\theta = 2n\pi , \tag{3.19}$$

where m is the number of round trips that the ray takes before it retraces back on itself and n is an arbitrary integer. We can also determine the FSR of this type of cavity by knowing the number of roundtrips and the spacing of the cavity mirrors.

$$FSR = \frac{c}{2dm} \tag{3.20}$$

The off-axis injection approach coupled with astigmatic mirrors results in a spot pattern on the mirror surfaces that is a Lissajous pattern with an effective path length that is as long as the on-axis ICOS approach, but since so many modes are excited, the free spectral range is reduced to a point where it is narrower than the exciting laser and the cavity appears to have a continuous transmission as a function of wavelength. Although astigmatic mirrors are difficult to obtain, they can easily be achieved in the lab by simply clamping a spherical mirror with a force sufficient to distort its figure.

From this point onward the analysis of off-axis ICOS is essentially the same as for the on-axis approach except that the contrast ratio of the cavity is reduced so much that there is no need to dither the cavity or to average the output intensity.

4 Experiments and Results

4.1 Cavity Setup and Mode Matching

In order to mode match the laser and the cavity we first had to profile the collimated beam that was produced by a Thorlabs Mitsubishi diode laser (ML725B11F) that emits laser at a wavelength 1310nm and is mounted on a Thorlabs TCLDM9 mount. The diode's temperature is controlled by a Thorlabs LDC 500. As is indicated in Figure 4.1 there is a linear relationship between the temperature and the wavelength as long as the current is set. The Current is controlled by a Thorlabs LDC2000 laser diode controller.

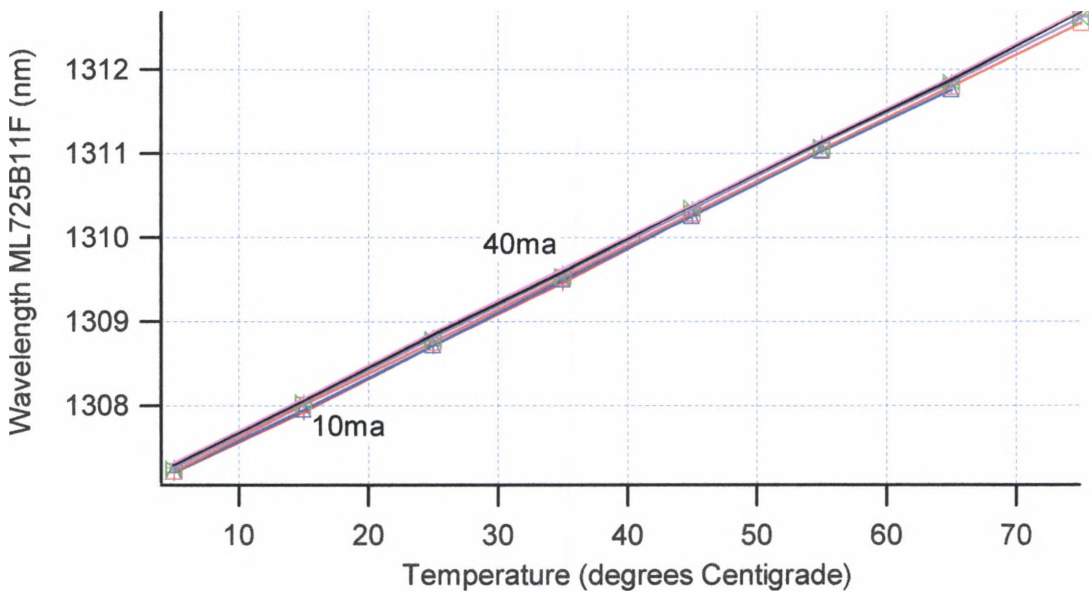

Figure 4.1 Wavelength of the Thorlabs diode laser as a function of diode temperature.

With the help of a Thorlabs free space fiber coupler the beam is then coupled into a single mode fiber with a collimating lens at the end of fiber and was mounted on a 3-D adjustable kinematic mount. The coupler position was adjusted in order to obtain an over 90% coupling efficiency.

Next we used the knife edge method to perform the beam profiling and determine the location and radius of the beam waist. To do this a razor blade was located at the end of the fiber on the optic axis. First a power meter and then a photo diode was located 2m from the fiber output on the optic axis. The razor blade was placed on a 2d translation stage enabling us to make very accurate measurements. The razor blade was moved slowly orthogonal to the beam and the orthogonal distance that intensity change was 8% to 92% was recorded. This process was recorded many times on the optics axis and the location of the laser blade was recorded each time. To ensure the accuracy of our measurements this process was also repeated with a Thorlabs Omega meter (an integrated spinning knife edge, detector, and readout) that measures the beam diameter and is very easy to use. The results were then fitted and the beams waist was determined $794\mu m$. Coincidently the beam waist of the cavity was calculated (based on the radii of curvature and the spacing of 0.862 m) to be $803\mu m$ which meant that a simple 1:1 mapping into the cavity would give good mode matching. The location of the laser beam waist was found to be -106cm from the output of the fiber which indicated that we have a virtual beam waist location. An optical imaging system was used to map this beam waist with a magnification of 1 into the center ringdown cavity. The first lens was a Newport's KBX088 and had a focal length of 1026.1mm measured at 1300nm.This lens was located 4cm from the output of the fiber (or 1 m away from the virtual waist). The second lens was actually the first cavity ringdown mirror from Los Gatos Research and was made out of silicon and had a focal length of -250cm. We developed a computer model that assisted us in determining the best position for our lenses to obtain the best mode matching. This lens/mirror was located 40cm from the first lens. To ensure that the beam

waist occurred exactly at the center of the cavity we performed another beam profiling experiment at 1550nm since the second mirror had a 50% transmission at that wavelength. The focal length difference between 1550 and 1310 is insignificant and the 50% transmission (as compared to 0.01%) allowed us to easily detect and profile the 1550 beam and hence verify the action of the cavity mirror on the beam. This experiment further confirmed that the cavity and the laser were mode matched. We were further able to confirm this after we set up the cavity as we will discuss in the future sections and observed many TEM_{00} modes and very few higher order modes with higher orders. Some of these modes are shown in Figure 4.2.

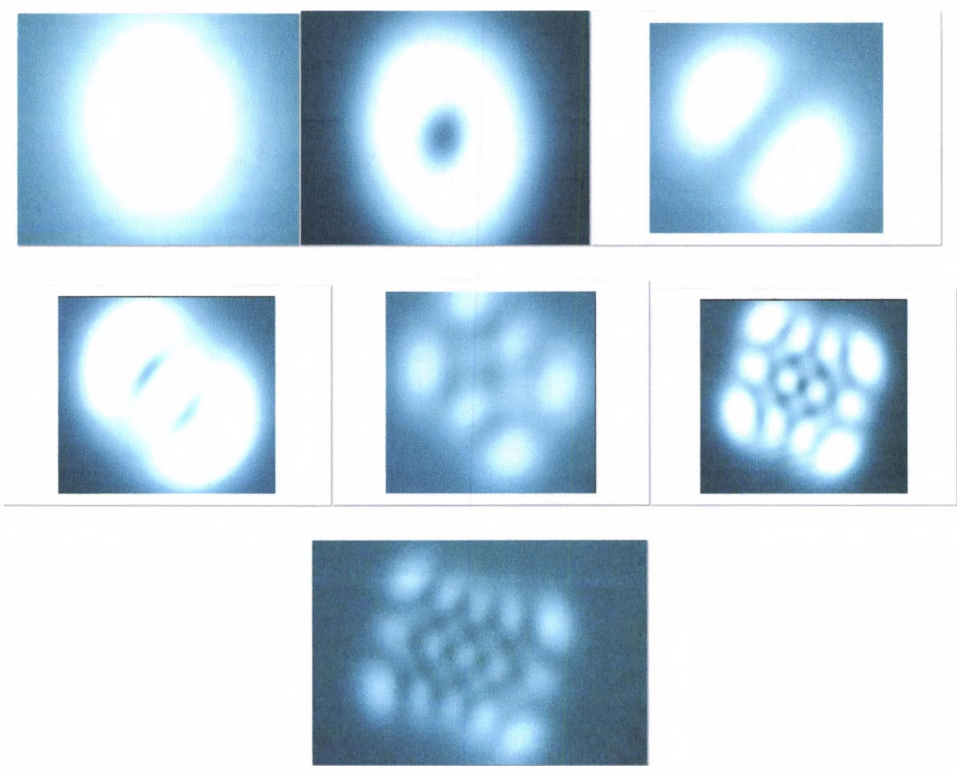

Figure 4.2 Photographs of actual modes excited in the cavity. A clear progression of the classic modes Hermite-Gaussian modes as described in Chapter 2 are seen as the alignment of the cavity and laser is moved away from ideal coupling to TEM_{00}.

4.2 Cavity Ringdown Spectroscopy

In order to setup the cavity we use the distances in between the CRD mirrors that were determined previously by mode matching section. The experiment setup is shown in Figure 4.3. The first step was to align the setup. We first placed pinholes centered at the both ends of the cell and observed the laser beam with an IR card and adjusted the steering mirrors until we observed the maximum intensity on the IR card. Next the pinholes were removed and the Los Gatos research labs Ringdown mirror located at the output was mounted inside the cavity. The mirror was then adjusted until its reflection was coincided back on the steering mirrors at the entrance of the cavity. The coincidence of this back reflection was observed with both IR cards and a Sensors Unlimited SU320 InGaAs infrared camera. The final cavity mirror was mounted an the entrance of the cavity and adjusted so that the reflection from it was again aligned with the incident beam. In this way the laser beam was centered in the cavity and both mirrors were set to be perpendicular to the beam.

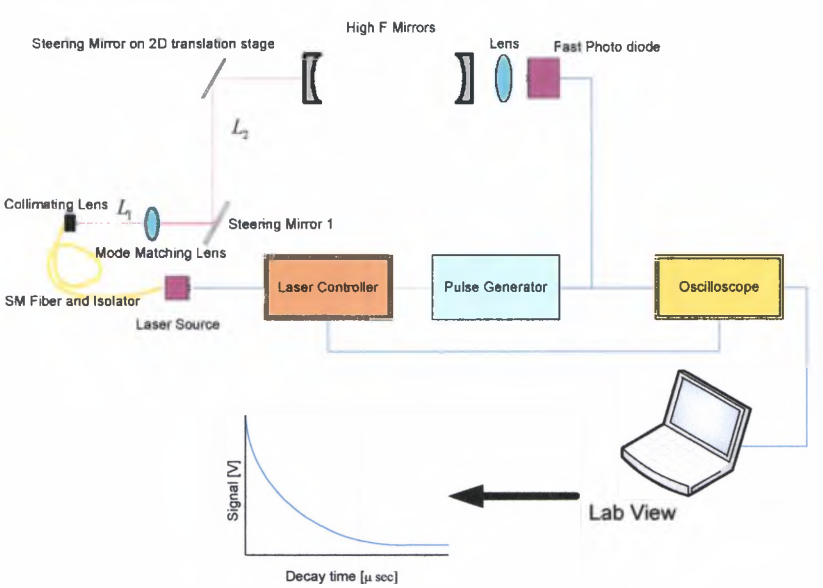

Figure 4.3 Schematic diagram of the cavity ringdown experiment.

To ensure that the alignment is complete and that the beam is exciting modes of the cavity, we placed the Sensors Unlimited IR camera at the output of the cavity and observed the transmitted light. Only very slight adjustment of the mirrors is required to insure that only TEM_{00} mode is transmitted by the cavity.

A fast lens f= 38.1mm (Newport KPX079) was used to focus the energy transmitted from the cell onto InGaAs photo diode with integrated transimpedance amplifier (Thorlabs PDA 255). The gain setting on the PDA 255 was adjusted so that the response time of the detector was $4\mu s$. As is shown in

Figure 4.3 the photodetector was connected to a model DG 535 Stanford Research digital delay generator. The delay generator was programmed to trigger when the diode current reaches a threshold value of 200 mV and kick the laser diode current controller with a step change in laser diode current. The energy build up took place when the cell's longitudinal modes and the frequency of the input laser were coincident. Triggering of the current controller then resulted in the laser and the cavity going off resonance, effectively decoupling the laser from the cavity so a ringdown event could be observed. In addition to kicking the laser current controller, the delay generator also triggered a Tektronix TDS3054B digital oscilloscope which recorded the ringdown signal from the photo diode.

A LabVIEW program was written to improve our data acquisition capability, assist us in analysis, and to help control our instruments. To obtain spectra, the laser frequency was changed manually in small step sizes (0.01nm) and was monitored with a Burleigh Wavemeter (WM-1000). The LabVIEW program took up to 50 sample decay times at each wavelength, averaged them and then fitted them to an exponential decay.

Figure 4.4 shows a cavity ringdown measurement of a single water absorption line in room air. The ringdown time on line center was too short to measure with our detector bandwidth which illustrate the narrow dynamic range of CRDS.

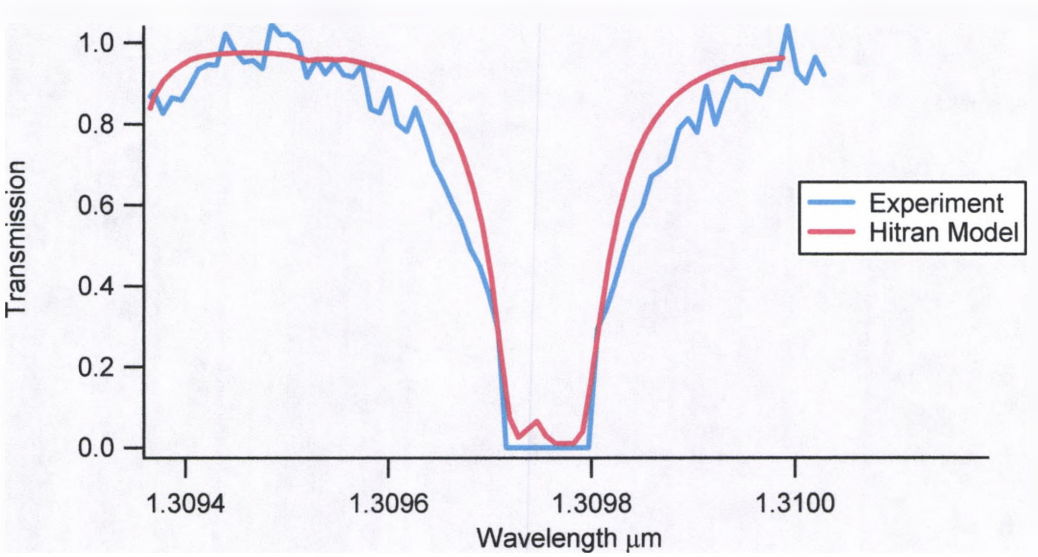

Figure 4.4. A cavity ringdown measurement of a single water absorption line. Unfortunately room air contained so much water that ringdown time was too short to measure with the current setup.

4.3 Integrated Cavity Output Spectroscopy (ICOS)

A New Focus model 6262 External Cavity Diode Laser (ECDL) was used as the tunable laser in this experiment. Two Newport super mirrors on a fused silica substrate, both with radii of curvature of 1m were used as cell mirrors. The mirror at the injecting end of the cavity was a Newport model 10CM00SR.70F which has a R=99.99%, while the mirror at the far end of the cavity was a mode 10CV00SR.70T which has a R=99.975%. Placement of a more transmitting mirror at the far end of the cavity makes

the detection easier while it needs to be considered that it also shortens the effective path length and therefore lowers the sensitivity of the experiment. The mirrors were placed 38.4 cm away from each other. The alignment of the cavity to the laser beam was achieved as in the CRDS setup. The energy exiting the cavity was focused into Thorlabs PDA255 photo detector with a f=38.1mm lens (Newport KBX139). The mirror at the output end of the cavity was mounted in a Thorlabs KC1-PZ piezoelectric kinematic mount. The piezoelectric mount was controlled by a Thorlabs MDT 693 3-axis piezoelectric controller that was driven by 3.5V peak-peak white noise signal noise generated by a model 33220A Agilent Technology function generator. The noise setting on the function generator was chosen randomize the cavity length over one FSR.

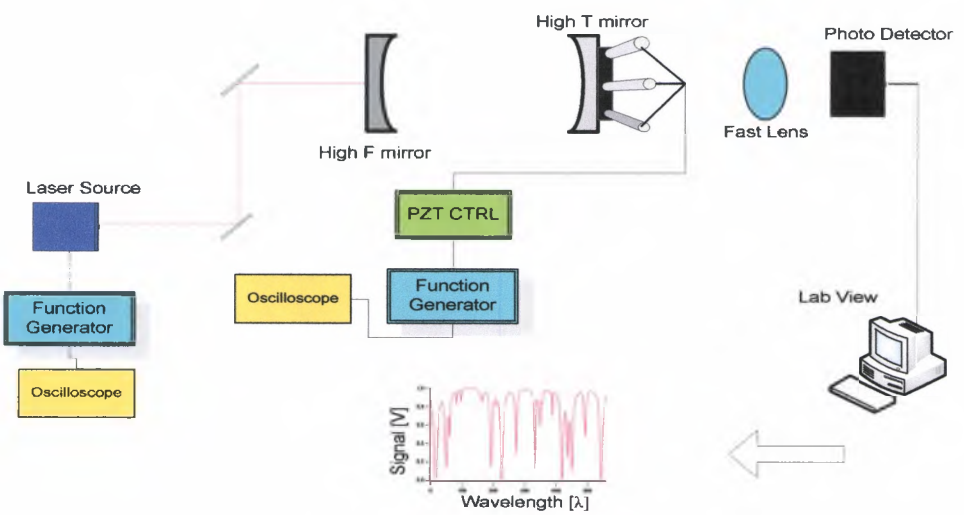

Figure 4.5 ICOS experimental setup. Note the similarity to the ringdown setup.

The laser was scanned at a speed of 0.01nm/sec on a sweeping mode. The step mode was avoided since it seemed to have mode hopping effects. The data was acquired using two different methods. First the photo detector was directly connected to the Tektronix

Digital oscilloscope and was triggered to collect and average 512 sweeps. A more sophisticated approach used LabVIEW and a National Instruments DAQPAD 6020F analog to digital converter enabled the averaging of more frequency sweeps and the collection of intensity data at 12 nits instead of the eight available with the oscilloscope. Beside the improved resolution, the communication with the A/D converter is much faster while every trace from the oscilloscope took nearly 1 second to transfer via GPIB when triggering overhead is included.

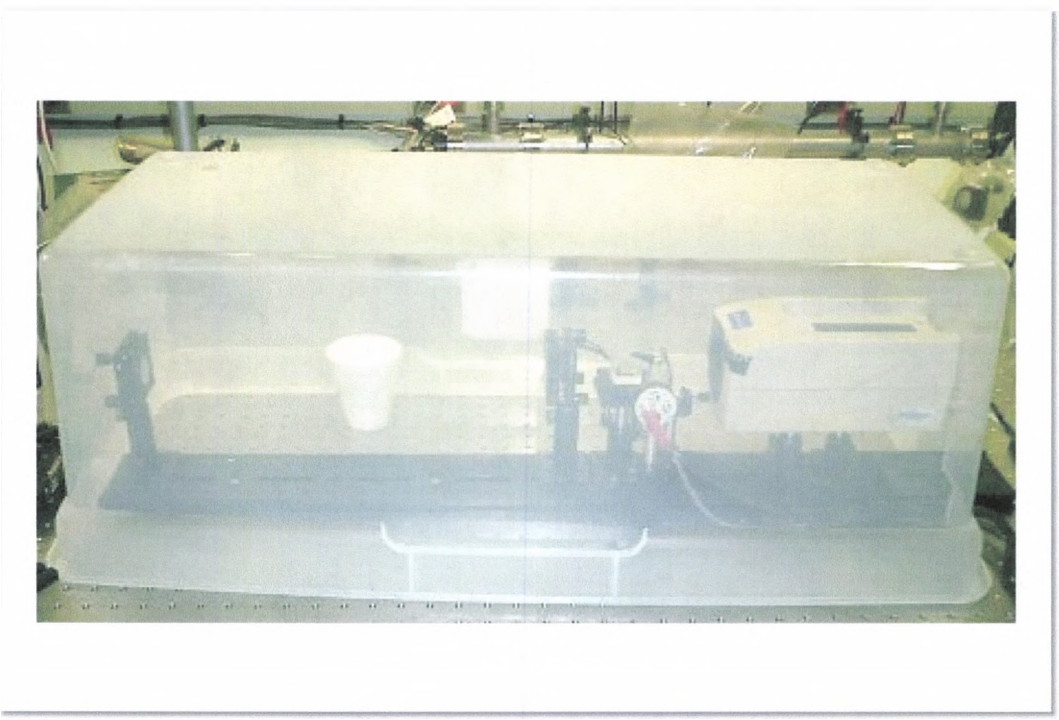

Figure 4.6 Photograph of the ICOS setup with a crude nitrogen purge setup that was used in an attempt to eliminate the observed water lines completely.

A photograph of the ICOS setup with a nitrogen purge box is shown in Figure 4.6. A spectrum of room air taken with the ICOS setup is in Figure 4.7. Due to a quirk of the New Focus laser wavelength output some of the adjacent data points have the same wavelength reading even though the laser was monotonically increasing the output

wavelength. In subsequent data sets we linearly interpolated between the starting and ending sweep wavelengths in order to generate the x-axis data.

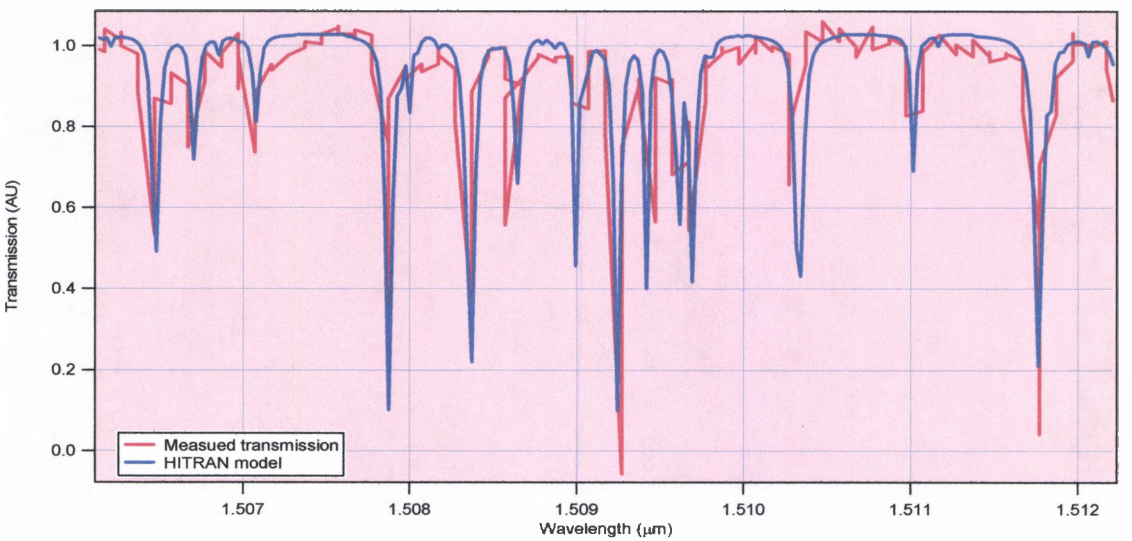

Figure 4.7 Measured ICOS and calculated HITRAN curves. The measured spectrum is plotted versus recorded wavelength.

4.4 Off-Axis ICOS

The setup of the Off Axis ICOS experiment was easier and simpler than both CRDS and ICOS. The same model 6262 External Cavity tunable Diode Laser that was used in the ICOS setup was used in these experiments. The last steering mirror before the cavity was mounted in a kinematic mount and placed on a 2-D translation stage so that the laser injection location and angle could be adjusted. The same two Newport super mirrors that were used in the ICOS experiment were used as cell mirrors and were placed 50.7cm from each other. The mirror at the injecting end of the cavity was a Newport 10CM00SR.70F which has a R=99.99%, while the mirror at the far end of the cavity was a Newport 10CV00SR.70T which has a R=99.975%. The initial alignment of the cavity

was conducted just like the ICOS and CRDS experiments. The major difference in the setup was that unlike the ICOS there was no use of piezoelectric mirror mounts. The setup is shown in Figure 4.8.

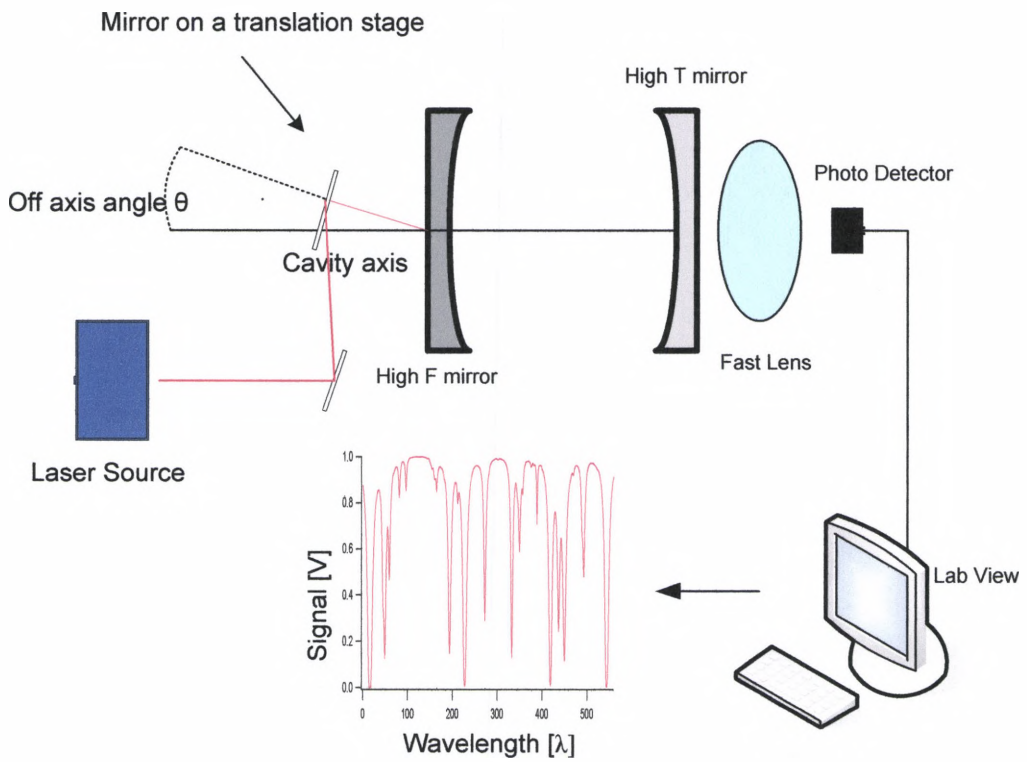

Figure 4.8. Off-axis ICOS setup. The setup is similar to CRDS and ICOS except that is even simpler and the alignment is less critical.

After completion of the alignment the steering mirror on the 2d translation stage was moved a few millimeters while the output of the cavity was being observed on the InGaAs infrared camera. Translation of the injection location combined with a small

amount of tilt away from normal incidence resulted in the pattern shown in the left part of Figure 4.9.

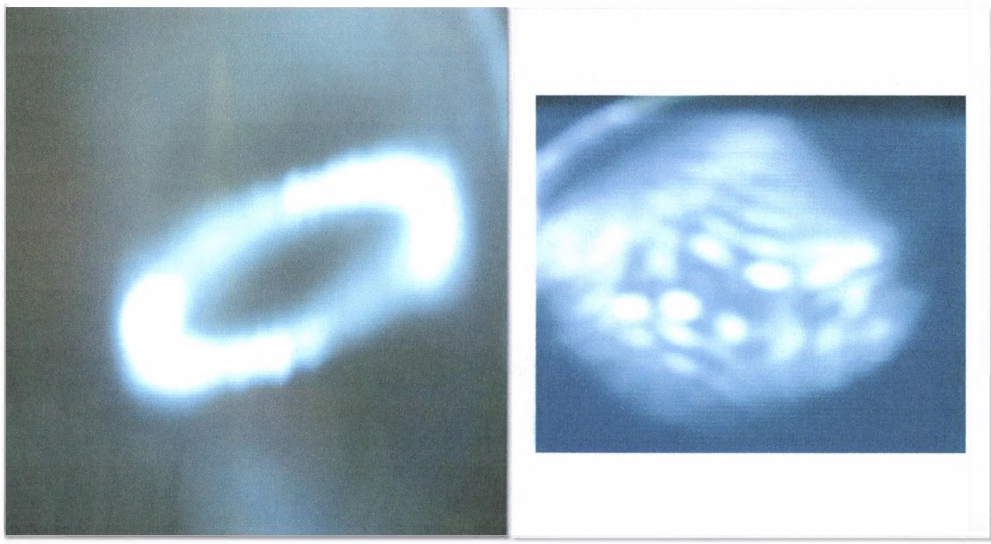

Figure 4.9. Photographs of off-axis ICOS cavity outputs. Reentrant cavity pattern from spherical mirrors (left) and Lissajous pattern from a slightly astigmatic mirrors (right).

The left pattern was due to and elliptical reentrant pattern on the spherical mirror surfaces. The right pattern was made by applying mechanical pressure on a spherical mirror by simply tightening the mounting screw in order to induce astigmatism in one of the mirrors. Gathering sufficient optical power on the photodiode was the most challenging part of this experiment. Not only is the intensity in the cavity lower in the off-axis ICOS setup, but it is also harder to focus the large output pattern onto the detector. It proved helpful to use a fast 2" diameter, f=38.1mm Newport KBX139 lens to focus the cavity output onto the photodiode and increase the power of the laser.

The laser was scanned at a speed of 0.01nm/sec on a sweeping mode. The same National Instrument's DAQPAD 6020F was used and the LabVIEW program used in

ICOS experiment was modified and used to acquire data. This allowed us to obtain a graph of signal voltage vs. time. The predicted results that were modeled using the HITRAN program were then compared with our experimental results. Figure 4.10 shows a spectrum of room air measured with the OA-ICOS setup and a HITRAN comparison.

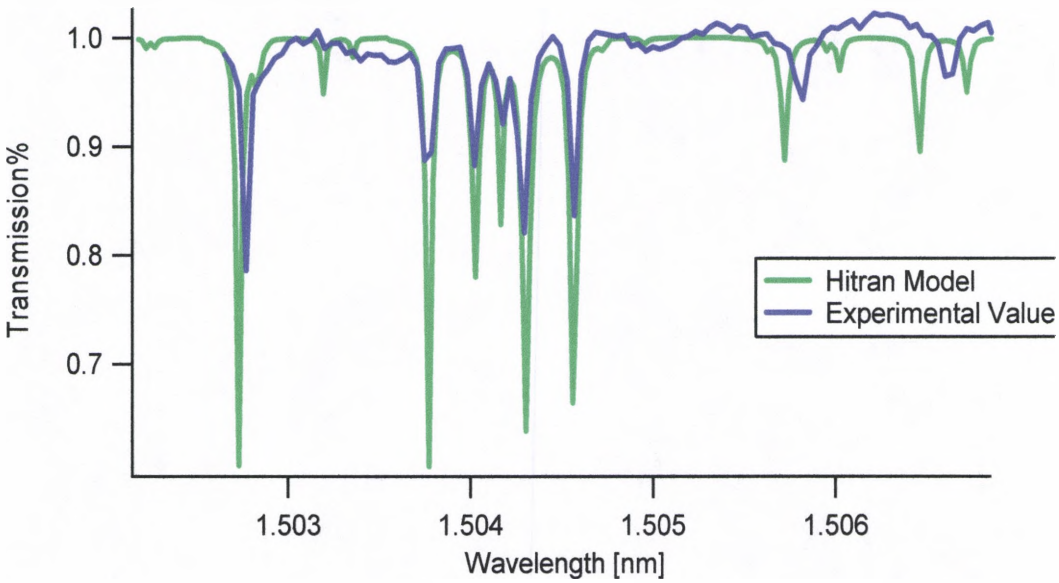

Figure 4.10. Room air transmission spectrum obtained with the OA-ICOS setup compared to the HITRAN model.

5 Summary and Conclusions

A comparison between the signal level of a single pass and the signal drop of the ringdown due to absorption of water molecules available in atmosphere was made. The signal level due to Cavity Ringdown Spectroscopy in this case was at least 100,000 times more than the signal drop in the case of the single path. Although this is sufficient to show that CRDS is the most sensitive method of spectroscopy that is used in this project, it does not permit us to determine the exact sensitivity of the CRDS in this project. Although the transmission line under study was really weak the very reflective cavity mirrors created a very long path length inside the cavity that caused a huge absorption that saturated the measurement as is indicated in Figure 5.1.

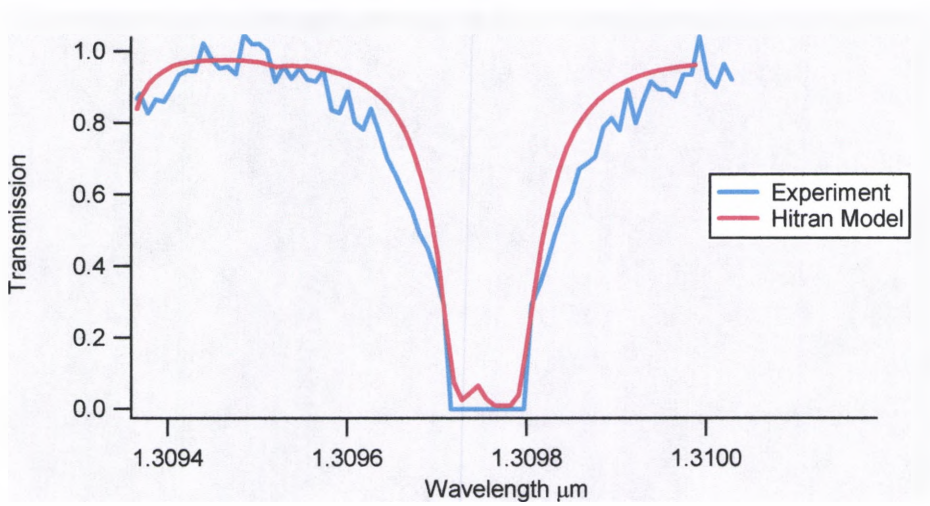

Figure 5.1. Saturated CRD signal.

The exact sensitivity of the CRD was not determined for two reasons. First reason was that the Mitsubishi laser's tuning range was very limited (2nm). In order to determine the exact signal drop we would need to be looking at even weaker absorption lines that the line shown in Figure 5.1 which would require more tuning. The second reason was that

this research was more oriented towards more robust means of sensitive spectroscopy such as ICOS AND OA-ICOS.

CW-CRDS has proven to be the most sensitive and at the same time the least robust method of spectroscopy that this study has looked into. The cavity and its mirrors need to be very stable. This makes CRDS less ideal for an environment that can introduce vibrations to the system. It is also important to mode match the cavity and the laser in CRDS while it is not the case in ICOS and OA-ICOS. The requirement for accurate mode matching takes away from the robustness of the system by adding additional components and sensitive optical alignment. CW-CRDS has a better spectral resolution than the pulsed CRDS. It is also less expensive particularly with the development of diode lasers.

Several absorption spectra of water molecules available in the atmosphere were obtained using the ICOS setup. All the absorption features studied belonged to very weak spectral features of water molecule and were modeled using the HITRAN program and data base. The signal drop when scanning across some of the water features using the ICOS method was compared to the signal drop when scanning across the same features in direct absorption setup. The signal drop due to absorption in the ICOS case in some instances was up to 58,000 times more than the signal drop in the case of a single pass direct absorption. This indicates the very sensitive nature of the ICOS method in detecting gases with weak absorption features. Being capable of detecting these weak absorption features also gives us more flexibility in the types of laser systems that can be used for this type of spectroscopy. This is very important in the cost saving sense. The same sensitivity levels were also measured when using an ICOS setup with a mirror spacing of 5cm. The system also proved to be very robust, compact, and promising

technique for future field applications. For example, vibrations introduced from the surrounding environment instead of posing a problem can be used as means to further randomize the cavity modes.

For a more precise analysis of the system it is essential to scan through the same wavelengths without the presence of the measured absorption features. Due to shortage in necessary equipment it was not possible to repeat the scan in vacuum or without the presence of water to make a better measurement of signal to noise ratio.

Several absorption spectra of water molecules available in the atmosphere were obtained using the OA-ICOS setup with different entrance angles and cavity length. The OA-ICOS signal level in most of our measurements was a factor of two or three less than the drop in signal in the case of ICOS. However, OA-ICOS is still significantly more sensitive than direct absorption. Out of the several different cavity lengths and entrance angles used in our settings the least sensitive setup had a signal drop 17,000 times more than the signal drop in single pass while the most sensitive system had a signal drop 28,000 times more than the signal drop in a single path direct absorption. The OA-ICOS is the easiest to setup and requires the fewest number of components among all the ringdown spectroscopy techniques. OA-ICOS is relatively inexpensive like ICOS. It has similar characteristics to ICOS as far as its robustness, light weight nature and mobility and is very capable in measuring gases with weak absorption features. It would have been preferred to make the same spectroscopy measurement of the same wavelength range in vacuum to get a better understanding of the system's background noise. This did not take place since we did not have the necessary equipment and would be a great starting point for future work.

6 Bibliography

1. Paul, J., Scherer, J., O' Keefe, A. and Lapson, L. , Anderson, J. , Gmachi, C. , Capasso, F. , Cho, A. , "Infrared cavity ringdown and integrated cavity output spectroscopy for trace species monitoring," , *SPIE*, Vol. 4577, pages 1-11, (2001).

2. Edited by Kenneth W. Busch, Marianna Busch, "Cavity-Ringdown Spectroscopy An Ultratrace-Absorption Measurement Technique," American Chemical Society, pp. 7-252, 1999.

3. O' Keefe, A., Scherer, J. , J. B. Paul and R. J. Skaykally, "Cavity Ringdown Laser Spectroscopy (CRDS): History, Development, and Applications", Chemical Reviews, Vol. 97, No.1, P. 25-51 (1997).

4. O' Keefe, A., Scherer, J. and Paul, J., "CW Integrated Cavity Output Spectroscopy," Chemical Physics Letters, Vol. 307, pages 343-349, 1999.

5. D. R. Herriott, H. Kogelnik, and R. Kompfner, "Off-axis paths in spherical mirror interferometers," Appl. Opt. 3, 523-526 (1964).

6. Joshua B. Paul, Larry Lapson, and James G, Anderson, "Ultrasensitive absorption spectroscopy with a high-Finesse optical cavity and off-axis alignment" Appl. Opt. Vol. 40, No.27, 4904-4910 (2001).

7. G. C. Bjorklund, "Frequency Modulation Spectroscopy: a new method for measuring weak absorption and dispersion", Optics Letters, Vol. 5, No. 1, 15-17 (1980).

8. Long. Sheng Ma, Jun Ye, Pierre Dube and John Hall, "Ultrasensitive frequency-modulation spectroscopy enhanced by a high-finesse optical cavity: theory and application to overtone transition of C_2H_2 and C_2HD", O. S. A. , Vol. 16, No.12, 2255-2268 (1999).

9. Christopher C. Davis, "Lasers and Electro-Optics Fundamentals and Engineering," Cambridge University, pp. 316-380, 1996.

10. H. Kogelnik, T. Li, "Laser Beams and Resonators," Applied Optics, Vol.5, No.10, pp. 1550-1556, 1966.

11. http://www.physicsdaily.com/physics/Transverse_mode

12. Wolfgang Demtröder, "Laser Spectroscopy basic concept and Instrumentation", Chapter 6.2, Springer Publishing co. 2nd Enlarged edition, 1998.

13. A. A. Kosterev, A. L. Malinovsky, F. K. Tittel, C. Gamchl, F. Capasso, D. L. Sivco, J. Baillargeon, A. Hutchinson and A. Cho, " Cavity ringdown spectroscopic detection of nitric oxide with a continuous-wave quantum-cascade laser", Applied Optics, Vol. 40, No. 30, p. 5522-5529(2001).

14. O' Keefe, A., "Integrated Cavity Output Analysis of Ultra-weak Absorption," Chemical physics lettres, Vol. 293, pages331,1998.

15. O' Keefe, A., Scherer, J. and Paul, J., "CW Integrated Cavity Output Spectroscopy," Chemical Physics Letters, Vol. 307, pages 343-349, 1999.

16. "Optical Electronics" Amnon Yariv, Chapter 4.1, Holt, Rinehart, and Winston, 1985.

17. "Optics" E. Hecht and A. Zajac, chapter 9.8, Addison-Wesley Publishing Co 1979.

18. R. Peeters, G. Berden, A. Apituley, G. Meijer, " Open-Path trace gas detection of ammonia based on cavity-enhanced absorption spectroscopy," Appl. Phys. B. Vol. 71, Pages 231-236, (2000).

19. Yury A. Bakhirkin, Anatoliy A. Kosterev, Chad Roller, Robert F. Curl, and Frank. Tittel, "Mid-infrared quantum cascade laser based off-axis integrated cavity output spectroscopy for biogenic nitric oxide detection," Appl. Opt. Vol. 43, No.11, 2257-2266 (2004).

20. D. R. Herriott, H. Kogelnik, and R. Kompfner, "Off-axis paths in spherical mirror interferometers," Appl. Opt. 3, 523-526 (1964).

21. Joshua B. Paul, Larry Lapson, and James G, Anderson, "Ultrasensitive absorption spectroscopy with a high-Finesse optical cavity and off-axis alignment" Appl. Opt. Vol. 40, No.27, 4904-4910 (2001).

22. D. S. Baer, J. B. Paul, M. Gupta, A. O' Keefe, "Sensitive absorption measurement in near infrared region using off-axis integrated cavity output spectroscopy", Appl. Phys. B (2002).

23. G. C. Bjorklund, M. D. Levenson, "Frequency Modulation(FM) Spectroscopy, Theory of Lineshapes and Signal-to-Noise Analysis", Appl. Phys. B. 32, 145-152(1983).

24. Philip C. D. Hobbs, "Ultrasensitive laser measurements without tears", Appl Opt. Vol. 36, No. 4, 903-920 (1997)